Methanol steam reforming behavior of sol-gel synthesized nanodimensional $Cu_xFe_{1-x}Al_2O_4$ hercynites

Sayantani Maiti[a], Dipak Das[a], Kamalesh Pal[a], Jordi Llorca[b], Lluís Soler[b], Sara Colussi[c], Alessandro Trovarelli[c], K. R. Priolkar[d], P. R. Sarode[d], K. Asakura[e], Md. Motin Seikh[f], Arup Gayen[a,*]

[a] *Department of Chemistry, Jadavpur University, Kolkata 700032, India*
[b] *Institute of Energy Technologies, Department of Chemical Engineering and Barcelona Research Center in Multiscale Science and Engineering. Universitat Politècnica de Catalunya, EEBE, 08019 Barcelona, Spain*
[c] *Dipartimento Politecnico, via del Cotonificio 108, Università di Udine, 33100 Udine, Italy*
[d] *Department of Physics, Goa University, Goa 403206, India*
[e] *Institute for Catalysis, Hokkaido University, Sapporo , Japan*
[f] *Department of Chemistry, Visva-Bharati University, West Bengal 731235, India*

Abstract

This work reports the outstanding catalytic activity behavior of sol-gel synthesized nanostructured $Cu_xFe_{1-x}Al_2O_4$ ($0.3 \leq x \leq 0.8$; named as CuFeAln, where n = 30, 40, 50, 60, 70 and 80) hercynites towards methanol steam reforming (MSR) for hydrogen generation. Based on the durability studies, we had categorized the higher Cu-doped hercynites (CuFeAl70 and CuFeAl80) as the more effective in regard to activity and stability (maintenance of a methanol conversion of ~80% with low CO selectivity of 2% after 50 h of continuous operation at 275 °C for CuFeAl80) when compared with the lower Cu-doped counterparts (CuFeAl30 and CuFeAl40). The specific surface area of all the materials was about 50 $m^2 g^{-1}$ and they had similar reduction characteristics as obtained from H_2-TPR analysis. The lower reducibility below 280 °C of CuFeAl70 and CuFeAl80 was correlated with the higher stability of these samples during time on stream operation. The powder XRD analyses had shown pure phase hercynite formation with the gradual increase of Cu-doping, while there occurred a phase segregation in the reforming atmosphere leading to the formation of metallic copper. High resolution microstructural analyses had confirmed single phase hercynite formation at nanoscale and a reduction of copper subsequent to ageing as well as certain growth of the copper metal particles (from ~5 nm to ~8 nm) corroborating the XRD studies. The surface features from in-situ XPS had also suggested formation of reduced copper species, which was much lower for the higher Cu-doped samples. Cu K edge XANES spectral analyses also pointed to lower occurrence of reduced copper in the aged samples of higher Cu-doped hercynites. The experimental findings had been explained on the basis of partial breakdown of the spinel lattice structure leading to the formation of CuO, followed by its reduction to metallic copper nanocrystallites in the MSR atmosphere. A definite ratio of the reduced to oxidized copper species was maintained with time on stream and this caused nearly stable conversion behavior of the catalysts in methanol reforming.

Keywords: *Copper-doped hercynite; Sol-gel; Methanol steam reforming; Hydrogen generation; Time-on-stream activity behavior*

---

*Corresponding author; e-mail: agayenju@yahoo.com, arup.gayen@jadavpuruniversity.in
Ph: +91-33-2457-2767; Fax: +91-33-2414-6223

Introduction

Fuel cells are energetically efficient, not limited by the thermal efficiency of the Carnot cycle, and ecofriendly i.e., having minimum environmental impact making them suitable alternatives to fulfill the energy requirement for the coming generation. Moreover, they remain silent during operation, involve no moving parts and hardly emit hazardous compounds to the atmosphere [1, 2]. More specifically, polymer electrolyte membrane fuel cells (PEMFC) are suitable devices for small scale power generation as well as transport applications [3]. Apart from the issues of overcoming hydrogen storage and transportation, it is a prerequisite to produce nearly CO free (<10 ppm) hydrogen as fuel for PEMFC applications [4, 5]. This is because of the fact that the Pt-based catalyst at the anode gets deactivated by CO, a fuel cell poison, at concentrations exceeding a few parts per million [6]. The steam reforming reactions have been indicated as effective means for on-board hydrogen generation [7–9]. In comparison to the other sources, hydrogen production from methanol steam reforming (MSR) is a favorable solution due to its various advantages for low-temperature applications [5, 10, 11].

Apart from methanol steam reforming (Eq. (1)), hydrogen is generated via two parallel reaction pathways; thermal decomposition of methanol (MD; Eq. (2)) and water gas shift reaction (WGS; Eq. (3)) [11, 12]:

$$CH_3OH + H_2O \rightarrow 3H_2 + CO_2 \qquad \Delta H^0 = 49.7 \text{ kJ mol}^{-1} \qquad (1)$$

$$CH_3OH \rightarrow 2H_2 + CO \qquad \Delta H^0 = 90.2 \text{ kJ mol}^{-1} \qquad (2)$$

$$CO + H_2O \rightarrow H_2 + CO_2 \qquad \Delta H^0 = -41.2 \text{ kJ mol}^{-1} \qquad (3)$$

Transition metal oxides with spinel structure are very interesting materials due to their fascinating physical properties that include high mechanical and thermal stability, low surface acidity and high ability of cation diffusion and practical usefulness as magnetic materials, semiconductors, pigments, catalysts, refractory materials or as model systems to understand

the relative stabilities of cations in voids [13]. Various spinel group materials are reported to exhibit promising activity towards water gas shift [14]; steam reforming of dimethyl ether [15-19], ethanol [20-22] and methanol [23-36]. Hercynite ($FeAl_2O_4$) is an important spinel oxide and we have shown that the stabilization of Cu^{2+} within the spinel lattice structure has beneficial effects in the MSR activity [35]. The trivalent metal ions, and specifically iron have the functionality to prevent Cu-sintering [27, 37]. The spinel based materials usually suffer from low surface areas caused essentially by the high calcination temperatures required for phase formation thereby restricting the active site availability [15-17, 33]. The material properties for effective catalytic performance can be improved through modifications of synthesis routes.

Preparation of pure $FeAl_2O_4$ is a challenging issue probably due to the difficulty to stabilize the phase at a lower temperature [35, 38-40]. Its normal spinel structure can undergo inversion depending on the synthesis condition [41]. Dutta et al. have reported almost chemically ordered $FeAl_2O_4$ [38], while Fukushima et al. have shown its formation via a microwave synthesis route [42].

The method of preparation has a profound effect on the phase composition of the spinel and oxidation state of the active species for MSR. The $CuAl_2O_4$ prepared by coprecipitation shows good performance due to the formation of highly dispersed copper [23]. Presence of variable oxidation states of both copper and manganese in urea-nitrate combustion made Cu-Mn spinel is considered to be responsible for the good MSR activity [24, 25]. While the reduced form of Cu-Mn spinel oxide is reported to be more reactive than the reduced Cu-Mn non-spinel mixed oxide by Fukunaga et al. [26]. Enhanced stability of Cu^+ over $CuFe_2O_4$ and $CuMn_2O_4$ spinels prepared by citric acid complex method contributes to a high methanol conversion in comparison to the commercial catalyst $Cu/ZnO/Al_2O_3$ [16]. Kameoka et al. [27] showed the spinel structure of $CuFe_2O_4$ as the determining factor for the

high MSR activity of $CuFe_2O_4/SiO_2$ prepared following an incipient wetness impregnation (IWI) method. Increased dispersion of copper formed via reduction of rod like $CuFe_2O_4$ contributes to a high MSR activity [28]. The activity of $Cu/ZnAl_2O_4$ synthesized via impregnation method is shown to be controlled by the spinel structure of $ZnAl_2O_4$ with highly stabilized Cu^+ species on the support surface [29]. Conrad et al. [34] showed that incorporation of Cu^{2+} in to $ZnAl_2O_4$ is very effective for MSR. The report of Xi et al. [30] have advocated for the simultaneous presence of the $CuAl_2O_4$ spinel phase and a tiny amount of CuO for the catalyst made via solid-phase method to exhibit an excellent catalytic performance in MSR. High surface area $CuMn_2O_4$ made via silica gel confined precipitation method [31], as well as the low surface area CuM_2O_4 (M= Mn, Fe, Al and La) spinels synthesized via solid state route [32] are also highly active MSR catalysts.

An earlier report showed the difficulty to synthesize pure hercynite via solution combustion method [39], but Cu-substituted $FeAl_2O_4$ could be prepared successfully following this facile method that is shown to exhibit promising activity for methanol steam reforming [35]. Cu-doped hercynites $Cu_xFe_{1-x}Al_2O_4$ (x= 0.3-0.8) were synthesized via sol-gel method and the detailed structural and magnetic properties have been reported earlier [40]. Here we report the MSR behavior of these Cu-doped hercynites with the aim of understanding the state of Cu and how this would affect activity and durability of the materials. A comparison of performance of these catalysts with combustion synthesized materials [35] indicate that this catalyst formulation can well compete with other methanol reforming catalysts.

Experimental

Preparation and characterization of materials

The details of synthesis for $Cu_xFe_{1-x}Al_2O_4$ spinels ($0.3 \leq x \leq 0.8$; named as CuFeAln, where n = 30, 40, 50, 60, 70 and 80) via sol-gel method using nitrate salts of copper, iron and aluminum and anhydrous citric acid (CA) as the combustion agent can be found in our earlier report [40]. Specifically, the preparation of $Cu_{0.4}Fe_{0.6}Al_2O_4$ (CuFeAl40) involved the combustion of $Al(NO_3)_3.9H_2O$, $Fe(NO_3)_3.9H_2O$ and $Cu(NO_3)_2.3H_2O$ with CA according to the molar ratio of 2:0.6:0.4:12. In a typical synthesis, stoichiometric amounts of nitrate salts were dissolved in millipore water (~10% (m/V)) to make a homogeneous solution in a beaker followed by the addition of diluted nitric acid (~20 vol.%) to prevent the hydrolysis of the salts. Then CA was added to reach the desired molar ratio (total metal : CA) of 1 : 4. The resulting solution was kept overnight at 70 °C under stirring condition, followed by an increase of temperature to 250 °C for evaporation to form the citrate gel. At the point of complete evaporation, the xerogel started to burn to produce a black colored fluffy precursor that was ground well and calcined subsequently at 700 °C for 20 h in air to get the spinel oxide. **Table 1** lists the nominal composition and name of the materials prepared. Wherever used the fresh or as-prepared form of the samples have been denoted with 'Fresh/AP' after its name.

The powder X-ray diffraction (XRD) data were recorded in a Bruker D8 Advance X-ray diffractometer using Cu Kα radiation (λ= 1.5418 Å) operating at 40 kV and 40 mA in the 2θ range of 10–100° using Lynxeye detector (1D mode) with a step size of 0.02° and a dwell time of 1 s per step. Average sizes of the catalyst crystallites were calculated from the line broadening of the powder XRD peaks using Scherrer's equation.

The BET specific areas, volume and size of pores were measured in a TriStar3000 porosimeter (Micromeritics, USA) by the adsorption/desorption of N_2 (Sapio, 99,99%) at 77 K. The surface areas were measured in the pressure range $0.05 < P/P_0 < 0.3$). Before each measurement, the samples were degassed at 150 °C in vacuum for 90 min.

The samples were characterized by means of temperature programmed reduction (H_2-TPR) analysis in a Micromeritics Autochem apparatus. Before TPR, each sample (0.04 g) was pretreated in air at 350 °C for 1 h in order to clean the surface from weakly adsorbed species. After cooling to room temperature, the flowing gas was switched to a mixture of 5% H_2 in N_2 and the temperature was increased up to 960 °C at a heating ramp of 10 °C min^{-1}. Hydrogen consumption was measured by a thermal conductivity detector (TCD).

The microstructural characterization by HRTEM was performed in a JEOL J2010F instrument equipped with a field emission electron source and operated at 200 kV. The point-to-point resolution was 0.19 nm, and the resolution between lines was 0.14 nm. The magnification was calibrated against a Si standard. No induced damage of the samples was observed under prolonged electron beam exposure. Samples were dispersed in an alcohol (Scharlau, 99.99%, synthesis grade) suspension and a drop of the suspension was placed over a grid with holey-carbon film. Images were not filtered or treated by means of digital processing, and they correspond to raw data.

The XPS (X-ray photoelectron spectroscopy) surface characterization was done for two selected catalysts pressed to self-consistent disk forms in a SPECS system equipped with an Al anode XR50 source operating at 150 mW and a Phoibos 150 MCD-9 detector under analysis chamber pressure below 10^{-7} Pa. The sample area analyzed was about 2 mm × 2 mm. The pass energy of the hemispherical analyzer was set at 25 eV and the energy step was set at 0.1 eV. The charge stabilization was achieved by using a SPECS Flood Gun FG 15/40. *In situ* MSR (carried out at ~300 °C and lasted 30 minutes at each condition) experiments were performed over the same catalysts in a reaction chamber connected to the XPS analysis chamber that allowed treatments up to 600 °C at atmospheric pressure and sample transfer without exposure to air. The in situ MSR treated samples have been named as 'MSR300'.

The temperature of the sample was measured with a thermocouple in close contact with the sample holder, which was heated with an IR lamp. Calcination treatments were performed under synthetic air (Praxair; 21% O_2 and 79% N_2). The occurrence of the reaction/ treatment during the *in situ* experiments was followed by an AMETEK mass spectrometer (by monitoring the masses in the range 0-100 amu). Gases were introduced by means of thermal mass flow controllers, while water and methanol were introduced by bubbling the appropriate amount of carrier gas Ar (Praxair; 99.999%) to attain steam to carbon ratio (S/C) of 1.1 (molar basis). The data were processed with the CasaXPS program (Casa Software Ltd., UK) in reference to C 1s binding energy (BE) values at 284.8 eV. The atomic fractions (%) were calculated using peak areas normalized on the basis of acquisition parameters after background subtraction, experimental sensitivity factors and transmission factors provided by the manufacturer.

X-ray absorption near edge structure (XANES) spectra at Cu K edge in copper- iron ferrites were recorded at room temperature (~25 °C) in the range –100 eV to +60 eV with respect to metal edge (8979 eV) in transmission mode on BL9C beamline at Photon Factory, Tsukuba, Japan. The photon energy was calibrated for each scan with the first inflection point of the absorption edge in Cu metal foil. Both the incident and transmitted photon intensities were measured simultaneously using ionization chambers filled with appropriate gases. The absorbers were made by pressing the fine powder samples into pellets of 10 mm diameter with boron nitride (Wako Company, >99%).

Test of methanol steam reforming

Details of the experimental set up for performing the MSR tests are reported elsewhere [43]. Before activity measurements, the as prepared catalyst powders were pressed at first into pellets of 12 mm diameter applying 10 tons of force exerted by a hydraulic press,

then the pellets of the sample were crushed and sieved to obtain particle sizes in the range 85–100 mesh. The materials in mesh form were tested in their as-prepared forms without any pretreatment. The steam reforming of methanol was performed under atmospheric pressure over 0.1 g of as-synthesized catalyst mesh loaded in a continuous-flow quartz micro-reactor (ID = 6 mm) placed in a vertical tube furnace in the temperature range from 200 to 300 °C using an evaporated pre-mixed methanol (Spectrochem, HPLC grade) and water (Millipore) solution (steam/carbon (S/C) ratio of 1.1 (molar basis) flowing at a rate of 0.6 mL h^{-1}) and nitrogen as carrier (and also as the internal standard) to reach a gas hourly space velocity (GHSV) of 30000 h^{-1} (molar ratio of methanol: water: nitrogen= 1:1.1:8.4 in the mixture). Durability in MSR of the finalized catalyst materials were also tested and the samples collected after the ageing treatment have been named as 'Aged' sample. Analysis of the reaction compositions was carried out by an online Agilent 7890A gas chromatograph (GC) equipped with a polar Porapak Q and a molecular sieve 5 Å columns, a thermal conductivity detector (TCD) and a flame ionization detector (FID). All the gases used here were of UHP quality (purity > 99.99 %) and supplied by Chemix Speciality Gases, Bengaluru.

Since methanol was not introduced into the GC, conversion was calculated by performing a carbon balance. The methanol conversion (X_{MeOH}) and CO selectivity (S_{CO}) were defined by the following equations:

$$X_{MeOH} = \frac{n_{CO2} + n_{CO}}{n_{MeOH}} \times 100 \qquad (4)$$

$$S_{CO} = \frac{n_{CO}}{n_{CO2} + n_{CO}} \times 100 \qquad (5)$$

Where n_{CO2} and n_{CO} are the flow rates (mol min^{-1}) of CO_2 and CO, respectively in the dry reformate, and n_{MeOH} is the flow rate of methanol (mol min^{-1}) in the liquid mixture. As CH_4 or any other carbon containing species were never detected in our experiments therefore we considered only the mole of CO and CO_2 for the calculation of conversion and selectivity.

Mole (n) of each of the component gases were calculated by using the known flow rate of the internal standard (N_2) and the vol.% of N_2 and the other components of gas sample obtained from GC analysis by using the following equation.

$$n = \left(\frac{V_{N2}}{v_{N2}} \times v_p \right) / 22400 \qquad (6)$$

Where V_{N2} is the flow rate (mol min^{-1}) of N_2, v_{N2} is the vol.% of N_2 and v_p is the vol.% of a component 'p' of the gas sample obtained from GC.

The gas sample from the reactor was analyzed once steady state was reached at a particular temperature, approximately 50 min after reaction. Three gas samples were analyzed at each temperature which gave either same or similar (within 1-2 %) conversion values and the last GC data were used as the steady state value. The reproducibility of experimental data was verified by performing catalytic tests under the same reaction conditions and the experimental error was estimated to be within 3 %. The equilibrium values of methanol conversion and CO selectivity were calculated using the software package HSC5.1 (Outokumpu).

Results and Discussion

BET surface area and porosity analysis

The specific surface area (SSA) of the materials is listed in **Table 1** along with the respective pore volume and pore sizes. The BET surface area as well as porosity characteristics of the materials is very similar. As expected, all the materials are mesoporous in nature as evident from the Type II nature of their adsorption isotherms (not shown here). No change is noticed on increasing the Cu-doping from 30 at.% to as high as 80 at.% in the hercynite lattice, all of them possessing a SSA of about 50 m^2 g^{-1} despite an increase in

crystallite size (see **Table 1**). This might be explained by a different agglomeration degree of the samples.

Table 1

Structural, morphological and reduction characteristics of $Cu_xFe_{1-x}Al_2O_4$ spinels.

Spinel composition	**Name**	**Scherrer size (nm)**		**Specific Surface Area (m^2 g^{-1})**	**Pore volume (cm^3 g^{-1})**	**Pore size (Å)**	**H_2 uptake (mL g^{-1})**
		Fresh	**Aged**				
$Cu_{0.3}Fe_{0.7}Al_2O_4$	CuFeAl30	6	5	49.5	0.383	239	115.1
$Cu_{0.4}Fe_{0.6}Al_2O_4$	CuFeAl40	8	8	49.5	0.407	255	116.4
$Cu_{0.5}Fe_{0.5}Al_2O_4$	CuFeAl50	13	12	47.9	0.404	249	106.0
$Cu_{0.6}Fe_{0.4}Al_2O_4$	CuFeAl60	16	16	48.4	0.409	252	112.5
$Cu_{0.7}Fe_{0.3}Al_2O_4$	CuFeAl70	19	18	47.7	0.461	259	98.0
$Cu_{0.8}Fe_{0.2}Al_2O_4$	CuFeAl80	20	18	52.2	0.519	270	117.5

H_2-TPR studies

The results of TPR analysis are reported in **Fig. 1**. The profiles show a series of hydrogen consumption peaks at low temperature, between ca 130 °C and 280 °C, and at medium temperature between 300 °C and 450 °C with a series of broader and less intense peaks (approximately between 500 °C and 950 °C) that become smaller at increasing copper loadings. Regarding the nature of these peaks, their attribution is not straightforward due to the presence of different reducible Cu and Fe species which are strongly interconnected on the catalysts, as inferred also from XRD analysis (no CuO or Fe_2O_3 species detected, see below). Moreover, on these systems very complex phenomena of ion migration and Cu-Fe

alloying induced by hydrogen spillover might take place together with isomorphous replacement effects [44, 45]. What can be observed is that at increasing copper loading the medium temperature peak increases significantly, at the expenses of all the other ones. Usually the reduction of Fe_2O_3 occurs above 400 °C [46-48]; in this case a strong interaction between Cu and Fe, resulting in the spillover of hydrogen, might speed up the reduction process of iron species and increase Fe reducibility. Overall, the total hydrogen consumption calculated in the whole temperature range (**Table 1**) is quite similar for all the samples, indicating a similar degree of reduction (78-88%, within the experimental error considering the theoretical Cu and Fe amount in the samples) for the Cu-doped hercynites, with the exception of $Cu_{0.7}Fe_{0.3}Al_2O_4$ which shows a slightly lower hydrogen consumption (73% of overall reduction). Anyway, what seems more important by looking at the TPR profiles is the lower reducibility below 280 °C of $Cu_{0.7}Fe_{0.3}Al_2O_4$ and $Cu_{0.8}Fe_{0.2}Al_2O_4$ (supported also by XPS and XANES results of aged samples), which might be correlated with, or even the responsible factor for the higher stability of these samples during time-on-stream operation at 275 °C (see **Fig. 3** in the following, and also XPS and XANES results). In addition, these two samples present the strongest Cu-Fe interaction as inferred from the amount of hydrogen consumed in the first TPR peak, which is much lower (15-20%) than the theoretical amount needed for the reduction of CuO to metallic Cu.

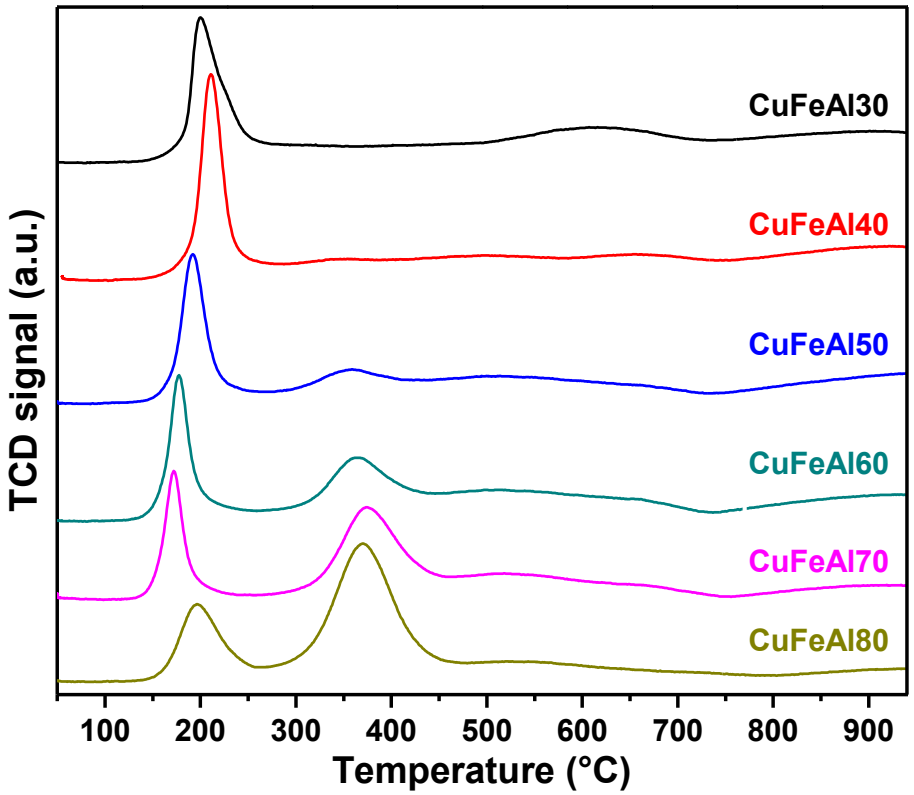

Fig. 1. H_2-TPR profiles of the CuFeAln (n= 30 to 80) samples.

Methanol conversion and CO selectivity

The methanol conversion and CO selectivity of the sol-gel synthesized copper substituted spinels for MSR are shown in **Fig. 2** together with the equilibrium values. All the materials are active in the investigated temperature range, 200-300 °C. The conversion increases sharply from < 30% at 200 °C with temperature up to ~ 275 °C. In an earlier study, we showed that pure hercynite shows almost no activity in the investigated temperature range [35]. So, it can be proposed that the reforming activity is solely due to Cu-incorporation in the hercynite lattice. All the materials, except CuFeAl30, show a methanol conversion of 90% or above (i.e., approaches the equilibrium value) at ~ 275 °C and on reaching 300 °C,

they give complete conversion (see **Fig. 2**). Throughout the temperature range tested here, CuFeAl30 shows the lowest activity behavior.

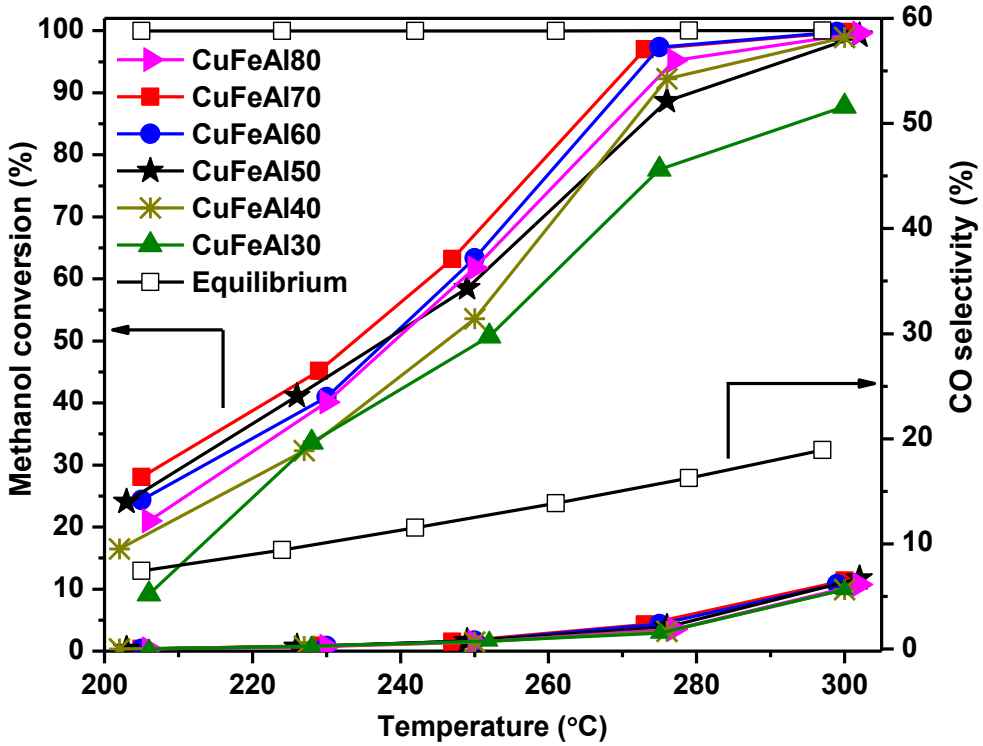

Fig. 2. Methanol conversion and CO selectivity of CuFeAln (n= 30 to 80) as a function of temperature at GHSV= 30,000 h^{-1} (S/C= 1.1).

No CO formation is detected at 200 °C (our GC can detect down to 10 ppm of CO); the CO selectivity exhibited by all the catalysts lays below the equilibrium values in the whole range of temperatures studied (see **Fig. 2** with values that are < 1% at 250 °C and increase slightly beyond this temperature (1.5-3% at 275 °C). Thus, the CO production routes, the methanol decomposition (Eq. (2)) and the reverse water gas-shift reaction (RWGS; $CO_2 + H_2 \rightleftharpoons CO + H_2O$), are also present together with the methanol steam reforming reaction at a higher temperature beyond 275 °C. These three reactions are all endothermic in nature and thus both kinetically and thermodynamically favored with the

increase in temperature. As the equilibrium conversion is very high, MSR is preferred over the CO production reactions. Above 275 °C, the catalysts show a sharp increase in CO selectivity (6-7%) that suggests the more prominent occurrence of CO formation reactions (MD and RWGS) at higher temperatures than at the lower temperatures.

It is difficult to make a comparison of catalytic performance of these Cu-doped hercynites with those of the literature reports because of the different experimental conditions. Nevertheless, the above catalytic data reveal noticeable gain in methanol conversion for the sol-gel synthesized hercynite samples (CuFeAl40 to CuFeAl80) when compared with the combustion synthesized catalyst CuFeAl10 and tested under the same reaction conditions as reported earlier [35]. In the former materials, the equilibrium conversion value is closely reached at a lower temperature of 275-280 °C compared to 300 °C for the latter catalyst. The CO selectivity values remain close to each other, ~3% for CuFeAl80 and ~4% for CuFeAl10 at ~280 °C. But it must be noted that the Cu-loading is much higher (40-80 at.%) for the sol-gel made samples and the particle sizes are also lower. Papavasiliou et al. [25] reported complete methanol conversion over Cu-Mn spinel catalyst at 240 °C when the CO selectivity remained around 3% and explained its increase at higher temperatures due to RWGS reaction. Most of the sol-gel made samples of this study gave similar methanol conversion and CO selectivity at a higher temperature of ~280 °C. This is interesting because a higher temperature generally favors the CO production routes besides reforming attributing to higher CO selectivity [25]. The question is whether the sol-gel synthesized materials can also sustain this activity behavior during continuous operation and obtain information about the phase stability of the samples under reforming atmosphere. To understand this we have performed time on stream (TOS) activity tests at 275 °C (when the

methanol conversion was nearly complete) for 50 h over two sets of SG materials at low and high Cu-loading (CuFeAl30 and CuFeAl40 vs. CuFeAl70 and CuFeAl80).

Durability study

The long term activity patterns of the four samples in the MSR atmosphere are shown in **Fig. 3**. The time gap between the two panels indicates overnight stay at the same reaction condition when no conversion data were collected. It was found that the higher copper doped samples CuFeAl70 and CuFeAl80 showed better conversion and stability than the lower Cu-doped samples CuFeAl30 and CuFeAl40, as expected. It was observed that the conversion exhibited by CuFeAl30 remained the lowest; it decreased continuously up to 32 h of operation and remained almost constant at ~62% up to 50 h. Although the CuFeAl40 sample maintains its maximum methanol conversion (~100%, similar to CuFeAl70 and CuFeAl80 samples) during first 8 h, it starts decreasing afterwards. Nevertheless, methanol conversion over CuFeAl40 (approaches ~68% up to 50 h) lies always above the conversion data of CuFeAl30. The highest conversion is exhibited by CuFeAl70 and CuFeAl80, the latter registers a little higher conversion than the former. In these cases, the conversion decreases to about 85% after 32 h, beyond which they maintain their conversion at about 78-82% upto 50 h. The CO selectivity values remain in the range ~ 1.2-3% for all the materials.

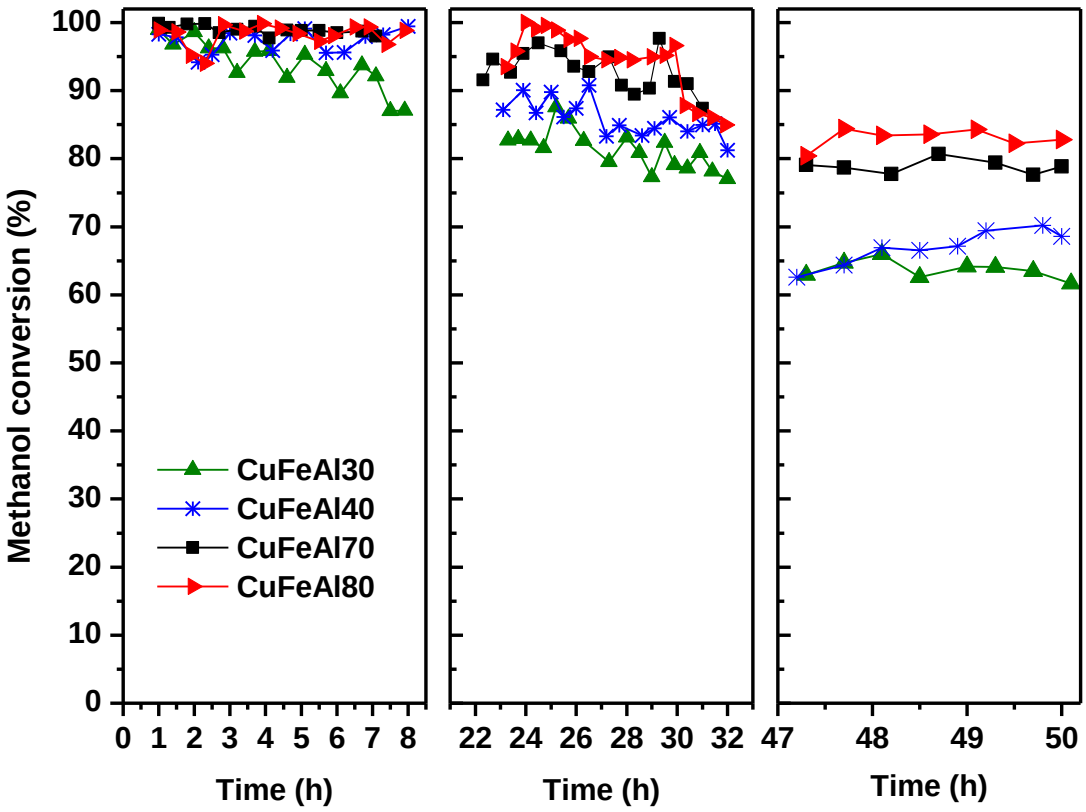

Fig. 3. The time on stream MSR activity patterns at 275 °C and GHSV of 30000 h^{-1} (S/C= 1.1)

In the following sections, the above catalytic outcomes have been explained on the basis of insights about the bulk phase analysis, the microstructure, surface elemental oxidation states and composition of fresh, aged and *in-situ* MSR treated catalysts and the near edge feature (XANES) of the various catalysts.

Powder XRD study

The powder XRD patterns of the two sets of materials in their as prepared forms are shown in **Fig. 4(a)**. The diffraction peaks correspond only to the cubic (Fd-3m) spinel structure in agreement with the literature report for the $CuAl_2O_4$ spinel (JCPDS PDF # 01–1153). No evidence of peak(s) due to the secondary phases of CuO, Al_2O_3 or Fe_2O_3 was

detected in the XRD patterns suggesting high purity of the crystalline phase formed. The average Scherrer size of the crystallites of the samples is listed in **Table 1**. The particles of the lower Cu-doped samples CuFeAl30 and CuFeAl40 are less than 10 nm in size, while the higher Cu-doped samples CuFeAl70 and CuFeAl80 are larger in size, ~20 nm.

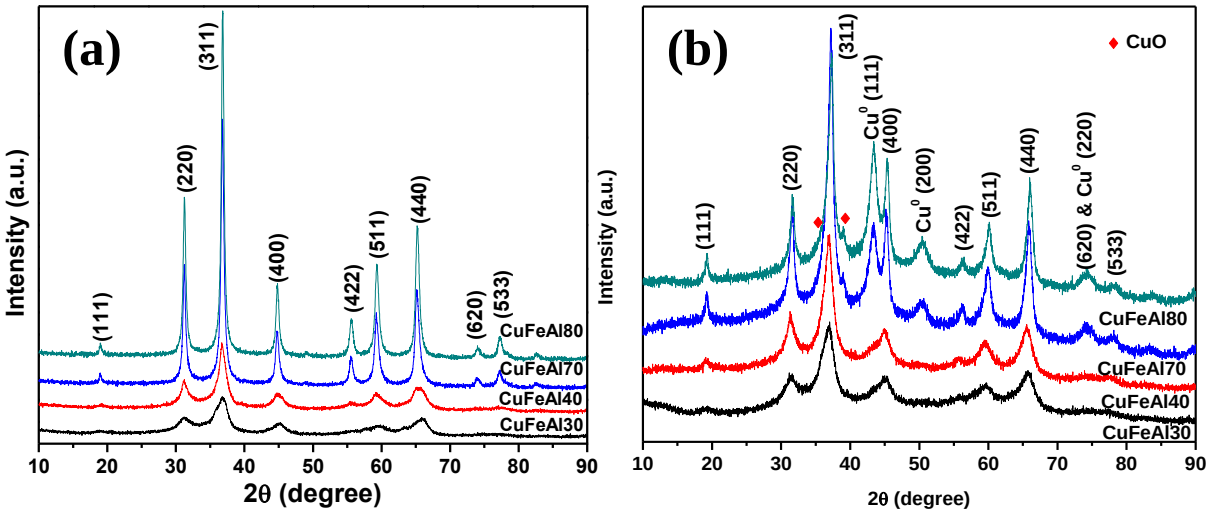

Fig. 4. The X-ray diffraction patterns of (a) as prepared and (b) aged (under MSR at 275 °C for 50 h) catalysts

Powder XRD analysis of the respective aged samples (after 50 h of MSR) show that the spinel phase remains as the major phase together with the formation of Cu-related phases, CuO and metallic copper (see **Fig. 4(b)**). While it is difficult to identify the presence of metallic copper in the lower Cu-doped samples CuFeAl30 and CuFeAl40, the formation of CuO (ICDD PDF # 89-2529) becomes clearly evident for the higher Cu-doped samples CuFeAl70 and CuFeAl80. Similarly, the metallic copper (ICDD PDF # 04-0836) formation is also very clearly evidenced from the diffraction patterns. It is also to be noted that the relative proportion of metallic copper is more than its oxide, a rough estimate of which was obtained from the intensity/area ratio of the diffraction peaks of the metal/ metal oxide and the spinel phases. The peak area ratio of Cu^0(200)/spinel(440) is calculated to be 0.24 for

CuFeAl70aged, which increases more than double to 0.52 in case of CuFeAl80aged. While the CuO(111)/spinel(440) peak area ratio is comparable (0.21) for CuFeAl70aged, and much low (0.21) for CuFeAl80aged. Interestingly, the particles size remain similar on ageing (see **Table 1**). It is evident that Cu is coming out from the lattice either in the form of CuO or metallic Cu. Thus one can anticipate simultaneous evolution of other phase(s) as the starting composition is pure and stoichiometric. The evidence of excess Al on particle surface is confirmed from our XPS studies discussed in the latter section. This Al is likely to be amorphous alumina or in AlO_x form and thus not detected in XRD pattern.

It thus becomes obvious that the sol-gel route is able to produce single phase copper doped hercynite with Cu-loading as high as 80 at.%, but this high Cu-loading is not sustained in the MSR environment and a multiphase composite of the spinel phase, copper oxide and metallic copper is formed. Despite this phase transformation, the particle sizes of the spinel phase after the ageing treatment remain essentially unaltered (see **Table 1**). The crystallite size for metallic copper is ~8 nm, whereas the CuO crystallite size is ~10 nm for both CuFeAl70 and CuFeAl80.

Microstructural analysis

The low-magnification TEM images of the fresh catalyst samples (not shown) show that they were constituted by small crystallites with mean particle size of about 10-20 nm. In general and in accordance with XRD results, the higher the Cu content the larger the crystallite particle size, although there was a wide size distribution in all cases. **Fig. 5(a-d)** show representative high-resolution transmission electron microscopy (HRTEM) and Fourier Transform (FT) images of selected areas of samples CuFeAl30, CuFeAl40, CuFeAl70 and CuFeAl80, respectively. The HRTEM images revealed clearly that the particles are completely crystalline, while the FT images show rings corresponding to multiple crystallites

randomly oriented. The spacing values recorded correspond well to the spinel structure in all cases. In **Fig. 5(c)**, the FT corresponding to the area enclosed in the white square shows an individual spinel crystallite oriented along the [111] crystallographic direction. In **Fig. 5(d)** the characteristic large spacing corresponding to the (111) crystallographic planes of the spinel structure are clearly visible.

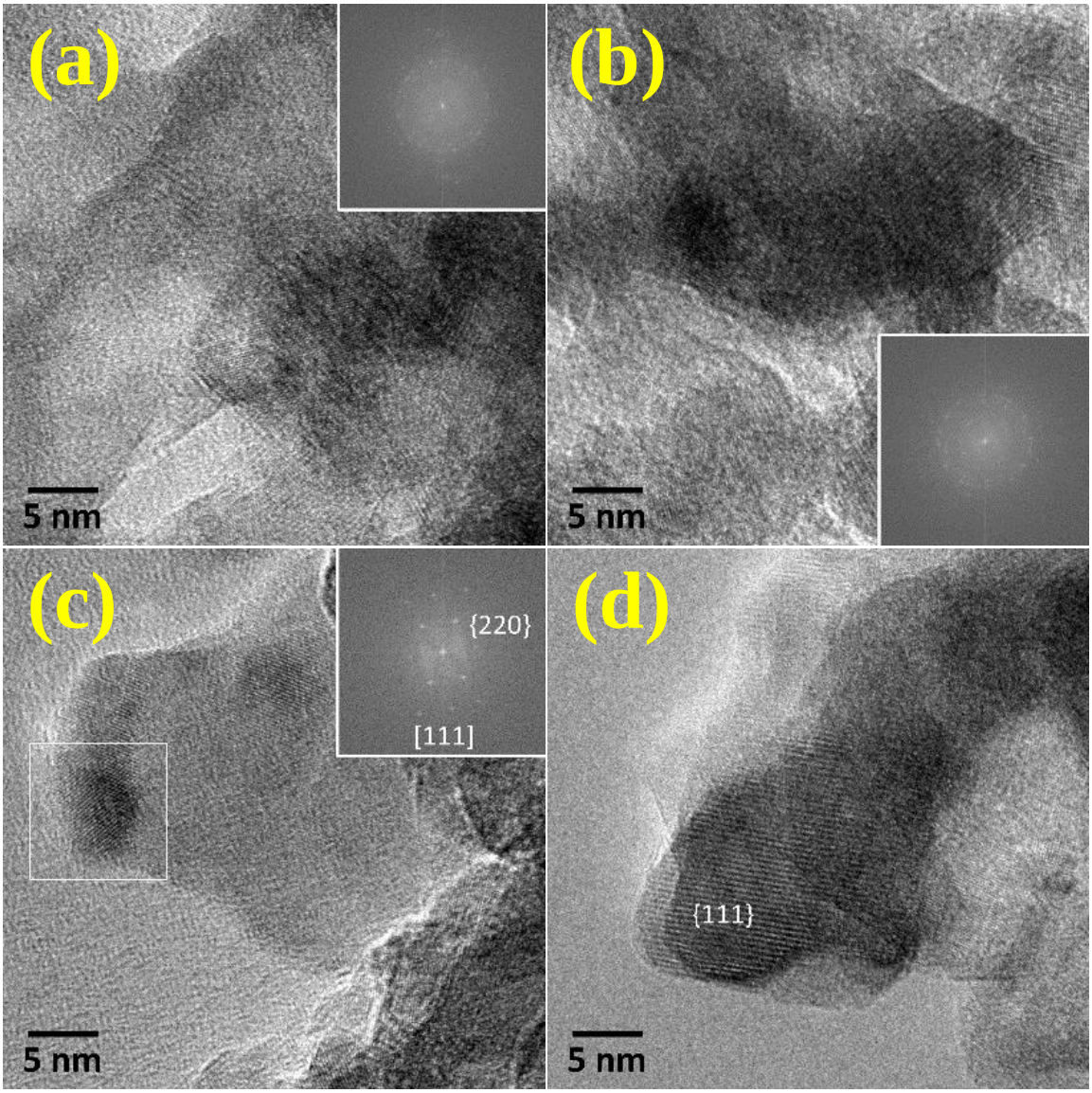

Fig. 5. HRTEM images of (a) CuFeAl30, (b) CuFeAl40, (c) CuFeAl70 and (d) CuFeAl80.

The samples exposed to MSR conditions for 50 h (the aged catalysts) show the formation of metallic Cu, being the segregation of Cu more evident as the Cu content in the

sample increased. **Fig. 6(a, b)** show low-magnification TEM images corresponding to the samples CuFeAl40aged and CuFeAl80aged, respectively. In both samples, presence of small nanoparticles with higher electron contrast was seen (some of them marked by white arrows). The size of these nanoparticles range from less than 5 nm in the sample with lower Cu content (sample CuFeAl40aged) up to 8 nm in diameter in the sample with the higher Cu content (sample CuFeAl80aged). The identification of the nature of these nanoparticles had been attempted by HRTEM, but only in the samples with higher Cu content this had been possible. **Fig. 6(c)** corresponds to HRTEM image recorded over the CuFeAl40aged catalyst in which it was not possible to study the nanoparticles properly given its low amount and/ or small size, and all the lattice fringes analyzed corresponded to the spinel structure. **Fig. 6(d)** shows a representative HRTEM image of the sample CuFeAl80aged. Several Cu nanoparticles are marked by arrows and the FT image of one of them is displayed, in which the spots at 2.08 Å and 1.80 Å corresponded well to the characteristic spacing of (111) and (200) crystallographic planes of metallic Cu. In **Fig. 6(e)** a detailed HRTEM image showing the structural relationship between the host spinel phase and the segregated metallic Cu nanoparticles is shown. According to the FT analysis, particles labeled "a" and "c" corresponded to the spinel phase whereas particles labeled "b" and "d" corresponded to metallic Cu. In "a", spots at 4.68 Å corresponded to the (111) crystallographic planes of the spinel structure. In "b", spots at 2.09 Å corresponded to the (111) crystallographic planes of Cu metal. In "c", the FT image corresponds to a spinel crystallite oriented along the [112] crystallographic direction, and in "d" the FT corresponds to a Cu particle oriented along the [110] direction. There is an intimate contact between both phases but there is no epitaxy or any other structural relationship between the spinel host phase and the segregated Cu phase.

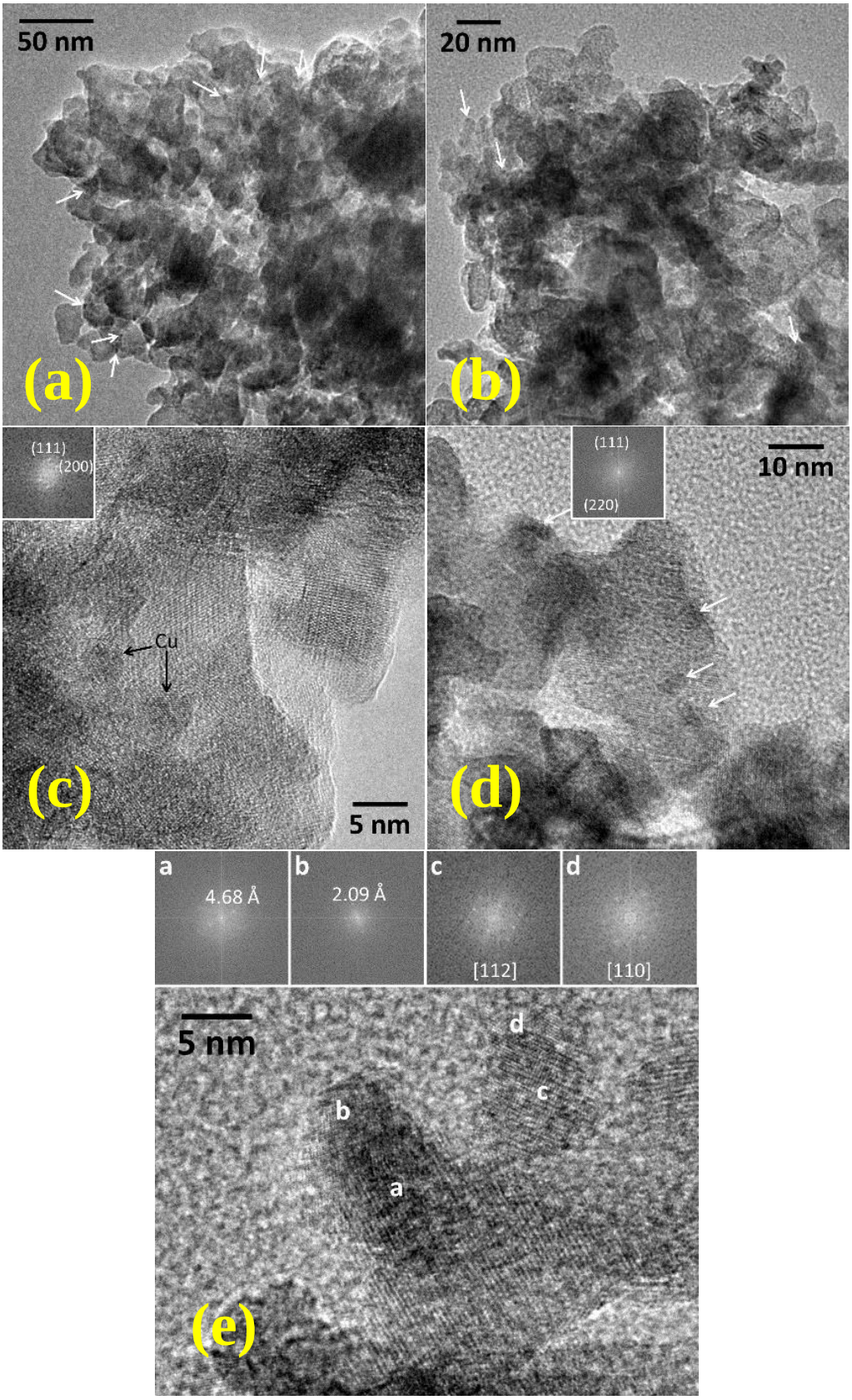

Fig. 6. Low-magnification TEM images of (a) CuFeAl40aged and (b) CuFeAl80aged and HRTEM images of (c) CuFeAl40aged and (d, e) CuFeAl80aged.

XPS studies

The Cu 2p core level spectra of CuFeAl40 and CuFeAl80 catalyst samples in their Fresh/ AP, aged and *in-situ* MSR treated (MSR300) forms are shown in **Fig. 7** and the data of surface analysis are listed in **Table 2**. The Cu 2p spectrum of the fresh/as prepared samples exhibit spin-orbit doublets centered at 933.5 and 953.5 eV and is accompanied by intense satellite bands separated by ~9 eV from the main spectral band that corresponds to Cu^{2+} species. In contrast, the in-situ MSR experiment clearly shows that Cu is reduced under reaction conditions. After MSR, the intensity of the satellite bands diminishes and a new band at lower binding energy emerges, which correspond to a reduced Cu species. Up to 88% Cu is present in the reduced state after the in-situ MSR test. From the CuLMM Auger lines (not included here) it is not possible to conclude on the exclusive presence of Cu^{+} or Cu^{0} in the samples subjected to in-situ MSR.

In addition to reduction of oxidized copper species, there is sintering of the Cu-phase during MSR; the amount of copper at the surface decreases from 4.6% to 3.4% for sample CuFeAl40 and from 8.8% to 6.3% in sample CuFeAl80 (see **Table 2**). This may be indicative of formation of Cu metal because a similar decrease is observed for the aged catalyst for which we have shown the prominent presence of metallic copper from both XRD and TEM analysis. In the aged samples, although the oxidation state of Cu cannot be properly assessed since the sample has not been treated under in-situ conditions, decrease in the amount of exposed Cu is similar.

Also, there is some segregation of Al towards the surface and the deposition of carbon during MSR (surface composition of both these components increase on ageing and after in situ MSR). The carbon depositions are obviously the highest for the ‘aged’ samples due to the longer exposure of the samples towards MSR atmosphere, 50 h in the reactor versus 30 min in case of in situ MSR test (MSR300). The difference in C 1s signal from the fresh (due to

adventitious carbon) and MSR300 and aged samples indicate a moderate carbon accumulation during methanol reforming experiments. Keeping in mind the very high surface carbon sensitivity of XPS signal, this is a good indication that carbon accumulation is not severe.

It is important to highlight that even if exactly the same tendencies are observed over both the CuFeAl40 and CuFeAl80 samples (see **Table 2**), the amount of reduced copper species after MSR is considerably lower in the CuFeAl80 sample with respect to the sample CuFeAl40, 56% vs. 88%. This definitely suggests that the substitutional Cu-ion is much more stable in CuFeAl80 than in CuFeAl40, which might be the determining factor for the TOS behavior observed. This conclusion is supported by TPR results, where CuFeAl80 presents a significantly lower reducibility below 280 °C with respect to CuFeAl40.

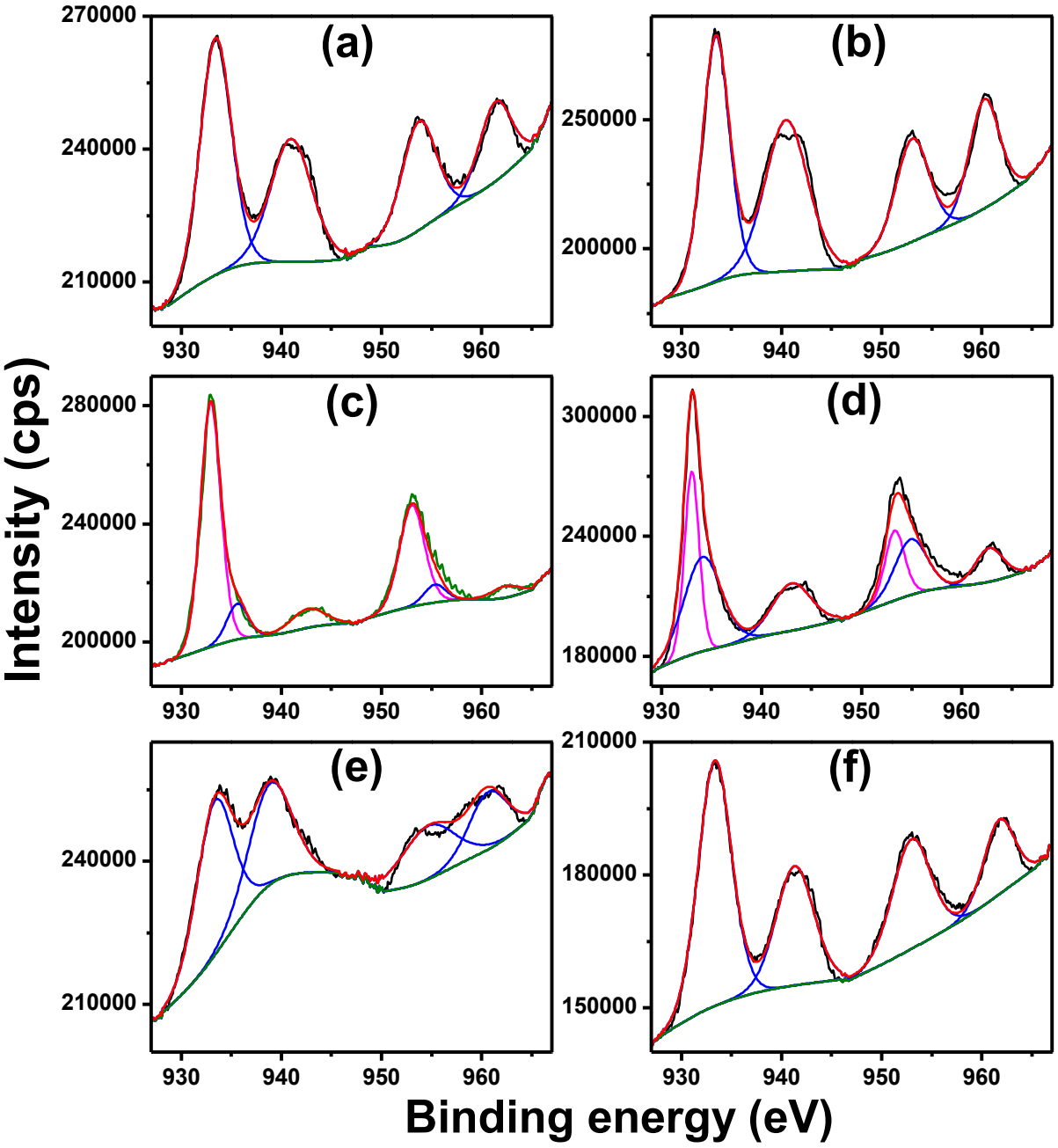

Fig. 7. Deconvoluted Cu 2p core level region of CuFeAl40 (left panels) and CuFeAl80 (right panels) in their (a, b) as prepared, (c, d) MSR300 and (e, f) aged forms. (Black: Experimental data; Red: Envelope; Olive: Background; Blue: Cu^{2+}; Magenta: Cu^{0}).

Table 2

XPS surface composition analysis of the CuFeAl40 and CuFeAl80 catalysts.

Sample	State	% atomic concentration					% Cu^{red}
		Cu	Fe	Al	O	C	
CuFeAl40	Fresh/ AP	4.6	6.0	27.2	57.9	4.3	0
	Aged	3.3	4.6	31.0	53.5	7.6	0
	MSR300	3.4	5.3	34.3	50.9	6.1	88
CuFeAl80	Fresh/ AP	8.8	4.2	29.0	53.3	4.7	0
	Aged	7.6	3.9	30.3	49.5	8.7	0
	MSR300	6.3	4.9	34.5	48.3	6.0	56

XANES studies

X-ray absorption fine structure spectroscopy has been used for the characterization of the as prepared and aged CuFeAl oxides. The analysis of the XANES region gives information on the oxidation state of the absorbing atom and on its coordination geometry of the absorbing metal ions. The normalized Cu K edge XANES spectra of the lowest (CuFeAl30) and highest Cu-doped (CuFeAl80) samples are given in the left side panels (see **Fig. 8 (a, b)**) along with the model compounds. Looking at the spectral profile of the aged sample it is evident that it exhibit the similar absorption features as the Cu^{2+} standard conveying thereby that there is a change in Cu-valence upon ageing. Such observations have been reported in literature for various copper and other compounds [49-54]. In the right side panels (see **Fig. 8 (c, d)**) the derivative spectra of all the four samples (in their AP and aged forms) are given along with those of the model compounds. It is clearly evident from the

similar appearance of the spectra that there occurs no change in Cu-valence in the as prepared samples irrespective of the Cu-content. But with ageing there is a noticeable change and CuFeAl80 and CuFeAl70 are bunched together, while CuFeAl30 and CuFeAl30 are bunched together. The additional intensity with respect to CuO sample's baseline below 8980 eV (which is absent in the AP samples) for all the aged samples indicates presence of reduced copper (Cu^0 and Cu^+) in all the samples.

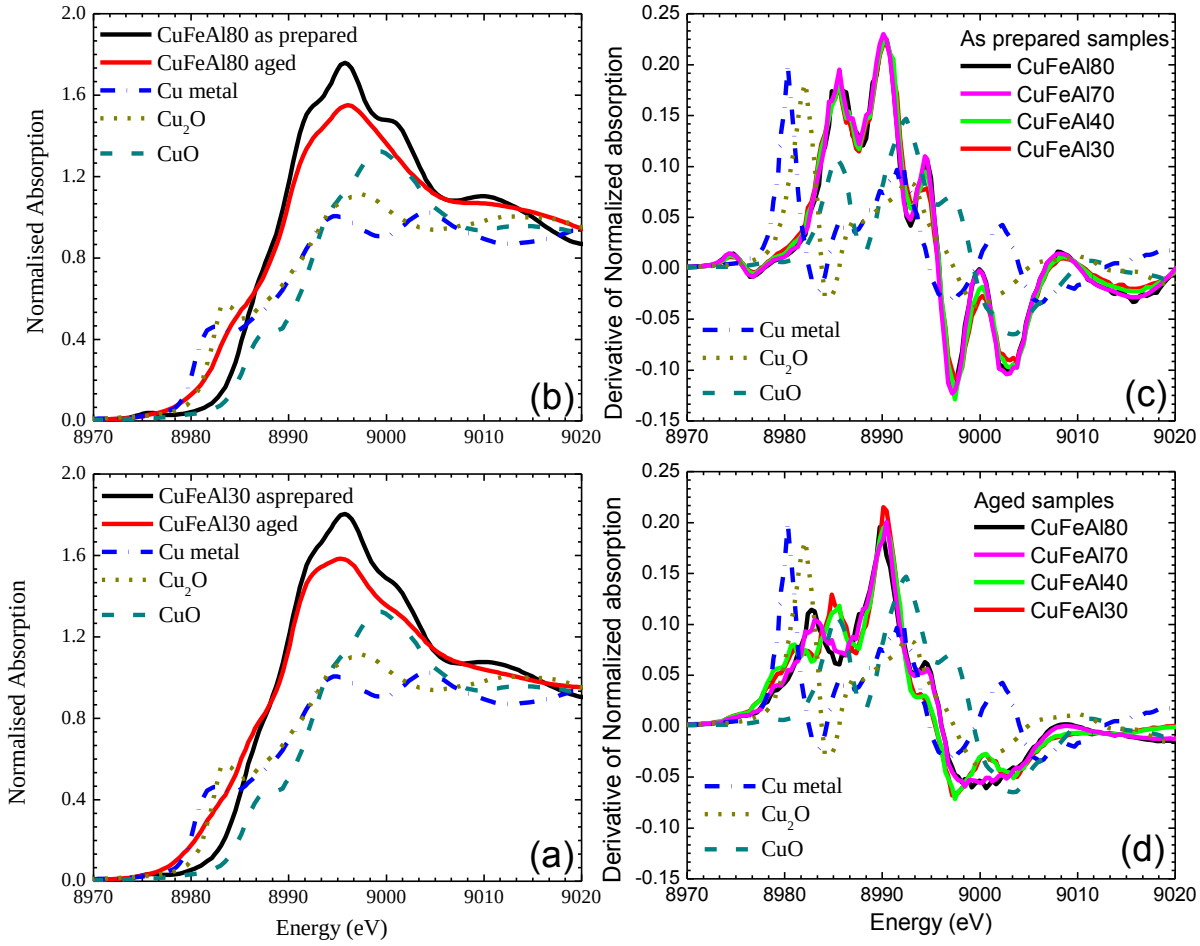

Fig. 8. Cu K edge XANES spectra of CuFeAl30 and CuFeAl80 samples (left panels (a, b)) and normalized derivative spectra of the four samples in their AP and aged forms (right panels (c, d)) along with the data of model compounds.

Fig. 9 shows the LCF (linear combination fitting) analysis for CuFeAl80 sample. The top panel (**Fig. 9(a)**) shows AP sample together with CuO. No combination of model compounds gives a better fit and so Cu is likely to be in +2 state. The inflection point or the first maximum in derivative spectrum of CuFeAl80 also matches well with that in CuO. Further the target spectra generated from principal component analysis of all the spectra of AP samples gives a reasonably good fit only to CuO indicating presence of Cu^{2+} in these as prepared samples (shown in the inset for CuFeAl80). In the lower panel (**Fig. 9(b)**), the LCF analysis is shown for the aged sample of CuFeAl80. It can be seen that a combination of 94% CuO (Cu^{2+}) and 6% of Cu (Cu^{0}) metal generates the experimental spectra quite well (see **Table 3**). A combination of 92% CuO (Cu^{2+}) and 8% of Cu_2O (Cu^{+}) also generates the experimental spectra equally well. The aged samples of CuFeAl70 is also characterized with large Cu^{2+} presence (89%) and small amount of reduced Cu-species (Cu^{0} ~5% and Cu^{+} ~6%). So, there is indeed a reduction of Cu in the aged samples. **Table 3** lists the relative proportions of various Cu-species in AP vis-à-vis aged samples obtained from XANES analysis and correspond to the best fitted data. For the aged samples of CuFeAl30 and CuFeAl40, there is more of Cu^{0} (23-25%) than Cu^{+} (6-7%), the predominant Cu-species is again Cu^{2+} (68-71%). Even if all the three Cu-species are included in the analysis, Cu^{2+} is found to be about 70%, the Cu^{+} percentage is about 3% to 4%, and Cu^{0} lies in the range 27% to 26%.

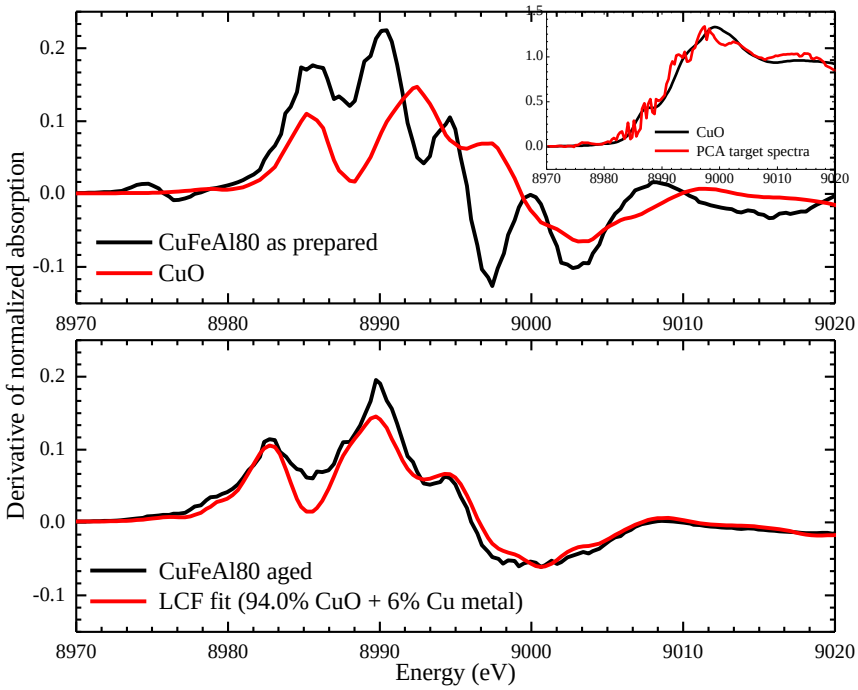

Fig. 9. LCF analysis for as-prepared (top panel) and aged (lower panel) samples of Cu80.

Table 3

Estimated proportions of various Cu-species for the as-prepared and aged hercynites.

Sample	Cu valence	AP (%)	Aged (%)
CuFeAl30	Cu^0	0	22.8
	Cu^+	0	6.7
	Cu^{2+}	100	70.5
CuFeAl40	Cu^0	0	24.7
	Cu^+	0	6.8
	Cu^{2+}	100	68.5
CuFeAl70	Cu^0	0	5.2
	Cu^+	0	6.1
	Cu^{2+}	100	88.7
CuFeAl80	Cu^0	0	6.0 (0)[a]
	Cu^+	0	0 (8.3)[a]
	Cu^{2+}	100	94.0 (91.7)[a]

a: the value in parenthesis corresponds to fittings with CuO and Cu_2O

Existence of metallic Cu in the aged samples is clearly evident from the XRD studies and has been corroborated strongly by the HRTEM studies. While XPS analysis remains essentially silent about its presence, the XANES analysis suggests the presence of metallic/ reduced copper in all the samples. The surface analysis after in situ MSR test truly supports Cu-reduction, but in different extents depending on the doping of copper. However, there is always a high possibility of the metallic Cu to get oxidized in air and hence it is understandable why we ended up with different findings on the presence of reduced copper species from the XPS and XANES analysis of the aged samples.

With the above findings on Cu-valence and their relative proportions on the surface of sol-gel derived hercynite catalysts, we can recall our earlier report on the combustion synthesized catalyst [35] for which the observed MSR activity behavior was explained to be strongly dependent upon the availability and ratio of partially reduced copper (Cu^{+}) to that of oxidized copper (Cu^{2+}) and relative proportion of both these two was attributed to be the key factor to exhibit a high MSR activity [31]. In general, a proper combination of reduced (Cu^{red}; Cu^{+} and Cu^{0}) and oxidized copper (Cu^{2+}) species plays a significant role in methanol steam reforming [32-34, 37, 39]. Strikingly, in case of the sol-gel synthesized samples we have noted that the higher Cu-doped samples (CuFeAl70 and CuFeAl80) show more pronounced diffraction peak due to metallic copper (see **Fig. 4(b)** corresponding to the aged catalysts) and these samples show comparatively better TOS activity behavior in respect to the lower Cu-doped samples (CuFeAl70 and CuFeAl80; see **Fig. 3**). Therefore, the presence of Cu^{0} species together with Cu^{2+} species (both as substitutional copper in the hercynite phase and as finely dispersed CuO) specifically in the higher Cu-doped samples CuFeAl70 and CuFeAl80 seems to be beneficial for a better (in comparison to our earlier reported solution combustion synthesized catalyst) and stable MSR behavior. The decrease in MSR activity during long term tests followed by its near constancy (from ~100% to ~80% beyond 32 h) may be

ascribed to be due to the following: (i) First, a portion of the ionically substituted copper comes out of the hercynite ($Cu_xFe_{1-x}Al_2O_4$) lattice phase and forms CuO in the course of ageing in the reforming atmosphere; (ii) Second, CuO formed so is subsequently transformed into Cu_2O and/or metallic Cu with the progress of reforming and (iii) Third, the Cu^0 thus formed is agglomerated thereafter to some extent. We believe that the relative occurrence of these phase transformations attributing to differences in the molar ratio of reduced to oxidized copper species is responsible for the observed time on stream behavior. Nevertheless, it is clearly evident that Cu^{red}/Cu^{2+} ratio is lower for the higher Cu-doped hercynites and it is the lowest for the most active sample CuFeAl80. The nearly stable conversion patterns beyond 32 h of TOS possibly suggest constancy of this ratio in the sol-gel derived copper ion substituted hercynite spinels of higher Cu-loading towards methanol steam reforming. It may also be pointed out that the role of Fe and Cu towards catalytic activity is indeed a tricky problem. It is well known that the oxides of these two metals are potential catalysts. However, the accentuation of catalytic activity of Fe containing spinel $FeAl_2O_4$ by replacement of Fe by Cu deserves a discussion on proper understanding of the role of Cu. Here we have given a plausible explanation of extraordinary activity of Cu in this catalyst. Cu predominantly appears in +2 oxidation state in oxides like hercynite and it is strongly Jahn-Teller (JT) active in both the tetrahedral and octahedral coordinations. The JT distortion leads to local lattice distortion. At lower Cu doping such distortion are localized. However, at higher Cu doping the lattice distortion may percolate through the cooperative distortion of the neighboring polyhedra. Such extended lattice distortion may modify the bond length locally enhancing the catalytic activity of the Cu-doped hercynites in methanol steam reforming.

Conclusions

The sol-gel method is shown to be a promising synthesis route for stabilizing the otherwise difficult to form $FeAl_2O_4$ phase through substitution of Cu at the Fe-site of hercynite. The nanostructured $Cu_xFe_{1-x}Al_2O_4$ ($0.3 \leq x \leq 0.8$) hercynites having specific surface area of about 50 $m^2\ g^{-1}$ show promising methanol steam reforming activity. Increase of Cu-doping enhances the MSR activity and the higher Cu-doped samples (x= 0.7 and 0.8) are more active and stable during the long term reforming tests compared with the lower Cu-doped samples (x= 0.3 and 0.4). The $Cu_{0.8}Fe_{0.2}Al_2O_4$ sample retains a methanol conversion of ~80% with low CO selectivity of 2% even after 50 h of continuous operation and it can be considered among the best candidates in copper based methanol reforming catalysts. The spinel lattice structure suffers partial breakdown in the reforming atmosphere following progress of the reforming reaction for a certain period of time and forms a composite of reduced (Cu^{red}; Cu^0 and Cu^+) and oxidized (Cu^{2+}) copper species. Nearly stable methanol conversion beyond 32 h of time-on-stream is caused due to the maintenance of the molar ratio of reduced to oxidized copper (Cu^{red}/Cu^{2+}) in the catalyst system. The highest activity of $Cu_{0.8}Fe_{0.2}Al_2O_4$ is not only due to its highest Cu-loading, but also the lowest Cu^{red}/Cu^{2+} molar ratio. The sol-gel made catalyst is also more active than the similar catalyst (but with much lower Cu-doping) made via solution combustion. More of copper (up to 80 at.%) can be doped for iron via the former method and hence they showed higher activity. The JT distortion of Cu^{2+} is expected to have crucial role behind the enhanced activity. These interesting features of the Cu-doped hercynites are expected to pave the way in designing more performant formulations in the future.

Acknowledgements

Financial support from the Science & Engineering Research Board (SERB), Government of India, by a grant (EMR/2016/001811) to AG and WB State fellowship to SM

and DST Special Grant to the Department of Chemistry, Jadavpur University in the International Year of Chemistry 2011 is gratefully acknowledged. JL is a Serra Húnter Fellow and is grateful to MINECO/FEDER project ENE2015-63969-R, GC 2017 SGR 128 and ICREA Academia program.

References

[1] D.S. Watkins, in: L.J.M.J. Blomen, M.N. Mugerwa (Eds.), Fuel Cell Systems, Plenum, New York, 1993, p. 493.

[2] J. Agrell, H. Birgersson, M. Boutonnet, I. Melián-Cabrera, R.M. Navarro, and J.L.G. Fierro, J. Catal. 219 (2003) 389–403.

[3] J.M. King, M.J. O'Day, J. Power Sources 86 (2000) 16–22.

[4] J.R. Rostrup-Nielsen, Phys. Chem. Chem. Phys. 3 (2001) 283–288.

[5] D.R. Palo, R.A. Dagle, J.D. Holladay, Chem. Rev. 107 (2007) 3992–4021.

[6] J. Larminie, A. Dicks, Fuel Cell Systems Explained, Wiley, New York, 2000.

[7] S. Sá, H. Silva, L. Brandão, J.M. Sousa, A. Mendes, Appl. Catal. B Environ. 99 (2010) 43–57.

[8] J.P. Breen, F.C. Meunier, J.R.H. Ross, Chem. Commun. 22 (1999) 2247–2248.

[9] J. Agrell, H. Birgersson, M. Boutonnet, J Power Sources 106 (2002) 249–257.

[10] Y. Choi, H.G. Stenger, Appl. Catal. B Environ. 38 (2002) 259–269.

[11] S.D. Jones, L.M. Neal, H.E. Hagelin-Weaver, Appl. Catal. B: Environ. 84 (2008) 631–642.

[12] B.A. Peppley, J.C. Amphlett, L.M. Kearns, R.F. Mann, Appl. Catal. A: Gen. 179 (1999) 21–29.

[13] J.C. Lashley, R. Stevens, M.K. Crawford, J. Boerio-Goates, B.F. Woodfield, Y. Qiu, J.W. Lynn, P.A. Goddard, R.A. Fisher, Phys. Rev. B 78 (2008) 104406.

[14] Y. Tanaka, T. Ukata, R. Kikuchi, T. Takeguchi, K. Sasaki, K. Eguchi, J. Catal. 215 (2003) 271–278.

[15] K. Faungnawakij, N. Shimoda, T. Fukunaga, R. Kikuchi, K. Eguchi, Appl. Catal. A Gen. 341 (2008) 139–145.

[16] Y. Tanaka, R. Kikuchi, T. Takeguchi, K. Eguchi, Appl. Catal. B Environ. 57 (2005) 211–222.

[17] K. Faungnawakij, R. Kikuchi, T. Fukunaga, K. Eguchi, J. Phys. Chem. C 113 (2009) 18455–18458.

[18] L. Oar-Arteta, A. Remiro, A.T. Aguayo, M. Olazar, J. Bilbao, A.G. Gayubo, J. Ind. Eng. Chem. 36 (2016) 169–179.

[19] L. Oar-Arteta, A. Remiro, A.T. Aguayo, J. Bilbao, A.G. Gayubo, Ind. Eng. Chem. Res. 54 (2015) 9722−9732.

[20] M.N. Barroso, M.F. Gomez, L.A. Arrua, M.C. Abello, Catal. Lett. 109 (2006) 13–19.

[21] H. Muroyama, R. Nakase, T. Matsui, K. Eguchi, Int. J. Hydrogen Energy 35 (2010) 1575–1581.

[22] F. Aupretre, C. Descorme, D. Duprez, D. Casanave, D. Uzio, J. Catal. 233 (2005) 464–477.

[23] M. Matsukata, S. Uemiya, E. Kikuchi, Chem. Lett. (1988) 761–764.

[24] J. Papavasiliou, G. Avgouropoulos, T. Ioannides, J. Catal. 251 (2007) 7–20.

[25] J. Papavasiliou, G. Avgouropoulos, T. Ioannides, Catal. Commun. 6 (2005) 497–501.

[26] T. Fukunaga, N. Ryumon, N. Ichikuni, S. Shimazu, Catal. Commun. 10 (2009) 1800–1803.

[27] S. Kameoka, T. Tanabe, A.P. Tsai, Cat. Lett. 100 (2005) 89–93.

[28] S.C. Yang, W.N. Su, S.D. Lin, J. Rick, J.H. Cheng, J.Y. Liu, C.J. Pan, D.G. Liu, J.F. Lee, T.S. Chan, H.S Sheu, B.J. Hwang, Appl. Catal. B Environ. 106 (2011) 650–656.

[29] P. Mierczynski, K. Vasilev, A. Mierczynska, W. Maniukiewicz, T. Maniecki, Top. Catal. 56 (2013) 1015–1025.

[30] H. Xi, X. Hou, Y. Liu, S. Qing, Z. Gao, Angew. Chem. Int. Ed. 53 (2014) 11886–11889.

[31] G. Marbán, T.V. Solis, A.B. Fuertes, Catal. Lett. 118 (2007) 8–14.

[32] Y.H. Huang, S.F. Wang, A.P. Tsai, S. Kameoka, Ceram. Int. 40 (2014) 4541–4551.

[33] Y.H. Huang, S.F. Wang, A.P. Tsai, S. Kameoka, J. Power Sources 281 (2015) 138–145.

[34] F. Conrad, C. Massue, S. Kühl, E. Kunkes, F. Girgsdies, I. Kasatkin, B. Zhang, M. Friedrich, Y. Luo, M. Armbrüster, G.R. Patzke, M. Behrens, Nanoscale 4 (2012) 2018–2028.

[35] S. Maiti, J. Llorca, M. Dominguez, S. Colussi, A. Trovarelli, K.R. Priolkar, G. Aquilanti, A. Gayen, J. Power Sources 304 (2016) 319–331.

[36] L. Oar-Arteta, A. Remiro, F. Epron, N. Bion, A.T. Aguayo, J. Bilbao, A.G. Gayubo, Ind. Eng. Chem. Res. 55 (2016) 3546−3555.

[37] S.T. Yong, C.W. Ooi, S.P. Chai, X.S. Wu, Int. J. Hydrogen Energy 38 (2013) 9541–9552.

[38] D.P. Dutta, G. Sharma, Mat. Sci. Eng. B 176 (2011) 177–180.

[39] R. Mistri, S. Maiti, J. Llorca, M. Dominguez, T.K. Mandal, P. Mohanty, B.C. Ray, A. Gayen, Appl. Catal. A Gen. 485 (2014) 40–50.

[40] S. Maiti, A.K. Kundu, O.I. Lebedev, P. Bera, C. Anandan, A. Gayen, M.M. Seikh, RSC Adv. 5 (2015) 83809.

[41] P.M. Botta, R.C. Mercader, E.F. Aglietti, J.M. Porto López, Scripta Mater. 48 (2003) 1093–1098.

[42] J. Fukushima, Y. Hayashi, H. Takizawa, J. Asian Ceram. Soc. 1 (2013) 41–45.

[43] D. Das, J. Llorca, M. Dominguez, S. Colussi, A. Trovarelli, A. Gayen, Int. J. Hydrogen Energy 40 (2015) 10463–10479.

[44] S.A. Theofanidis, V.V. Galvita, H. Poelman, N.V.R.A. Dharanipragada, A. Longo, M. Meledina, G.V. Tendeloo, C. Detavernier, G.B. Marin, ACS Catal. 8 (2018) 5983−5995.

[45] Q. Chen, S. Hu, J. Xiang, S. Su, L. Sun, Y. Wang, L. Zhang, H. Chi, Fuel Processing Technol. 146 (2016) 56–61.

[46] M. Zhu, S. Chen, A. Soomro, J. Hu, Z. Sun, S. Ma, W. Xiang, Appl. Energy 225 (2018) 912–921.

[47] H. Zhao, D. Mei, J. Ma, C. Zheng, Asia-Pac. J. Chem. Eng. 9 (2014) 610–622.

[48] P.R. Kidambi, J.P.E. Cleeton, S.A. Scott, J.S. Dennis, C.D. Bohn, Energy & Fuels 26 (2012) 603–617.

[49] S. Ebbinghaus, Z. Hu, A. Reller, J. Solid State Chem. 156 (2001) 194–202.

[50] C. Luadthong, P. Khemthong, W. Nualpaeng, K. Faungnawakij, Appl. Catal. A Gen. 525 (2016) 68–75.

[51] S. Riegg, A. Reller, A. Loidla, S.G. Ebbinghaus, Dalton Trans. 44 (2015) 10852.

[52] J.H. Choy, D.K. Kim, S.H. Hwang, G. Demazeau, Phys. Rev. B 50 (1994) 16631–16639.

[53] T. Tangcharoen, W. Klysubun, C. Kongmark, W. Pecharapa, Phys. Status Solidi A 211 (2014) 1903–1911.

[54] O. Saensuk, S. Maensiri, A. Bootchanont, E. Swatsitang, Microelectron. Eng. 126 (2014) 158–164.